# Advanced InP Photonic Integrated Circuits for Communication and Sensing

Shamsul Arafin, *Senior Member, IEEE*, and Larry A. Coldren, *Life Fellow, IEEE*

*(Invited Paper)*

***Abstract*—Similar to the area of microelectronics, InP-based photonic integrated circuits (PICs) in the optical domain as a counterpart are also seeing a clear exponential development. This rapid progress can be defined by a number of active/passive components monolithically integrated on a single chip. Given the probability of achieving low-cost, compact, robust, and energy-efficient complex photonic systems, there have been significant achievements made in realizing relatively complex InP-PICs in recent years. The performance of these complex PICs is reaching a stage that can enable a whole new class of applications beyond telecom and datacom. A great deal of effort from both academia and industry has made the significant advances of this technology possible. This development has resulted in a positive and profound impact in many areas including sensing, medical diagnostics, metrology, and consumer photonics. This review paper will mainly discuss the recent, in particular since 2012, progress and findings obtained out of current academic and industry research activities for InP-PICs. Major emphasis will be given to the high-performance and complex PICs that have been reported by the scientific community in this time period. A prospect for further development of this photonic integration in InP-platforms is also briefly described.**

***Index Terms*—Photonic integrated circuits, integrated optics, optical transceivers, optical filters, beam sweeping, optical phase-locked loop.**

## I. Introduction

OVER the past couple of decades, photonic integrated circuits (PICs) have delivered on much of the promise to provide reductions in size, weight and power over discrete solutions [1], [2]. In many cases, improvements in reliability, cost and even performance have been observed, although cost improvements require some significant production volume, and performance improvements only come if the integrated elements work well on the chosen integration platform. In fact, for some applications, some compromise in PIC performance may be tolerable, if improvements in the other mentioned aspects are achieved.

For active PICs, in which optical gain is required, such as those requiring lasers or semiconductor-optical-amplifiers (SOAs), it is most desirable to choose an integration platform that naturally provides gain, such as one based on a III-V semiconductor. For the low-loss or low-dispersion fiber optic windows at 1550 nm and 1310 nm, respectively, this III-V material platform has been based upon InP. Early InP-PICs containing both active and passive components at emission wavelengths of 1550 nm [3]–[5] and 1310 nm [6], [7] were reported and their potential for enabling applications in the area of fiber optics were also described.

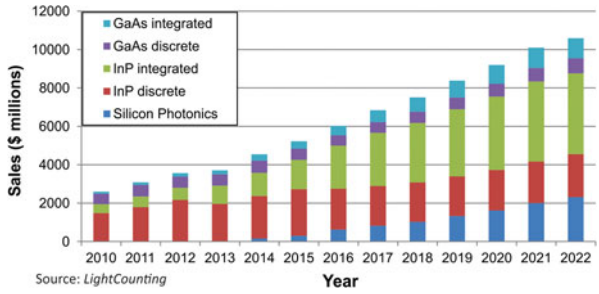


Fig. 1. A bar chart for the transceiver market history from 2010 and projection towards 2022. Reproduced with permission from [14].

Despite the great versatility of InP-based monolithic integration, a single waveguide platform cannot be utilized here for a single function. This often leads to restrictions in performance and applicability. However, this intrinsic problem can be circumvented by complex fabrication or additional regrowth steps [8].

The alternative to a pure monolithic InP-platform is to employ some sort of hybrid or heterogeneous solutions, in which a gain block or layer is incorporated with an otherwise passive PIC platform. This has been done by using a discrete InP-gain chip optically coupled to the passive PIC as well as by wafer bonding InP layers directly to the passive PIC. Microdisk lasers by Spuesens *et al.* [9], ring lasers by Liang *et al.* [10], multiwavelength AWG lasers by Kurczveil *et al.* [11], an optical transmitter by Srinivasan *et al.* [12] and a transceiver by Fedeli *et al.* [13] are some of the exemplary reports on InP-based lasers and SOAs integrated with silicon-photonics in recent years.

Although the PIC literature has been dominated by silicon photonics and these hybrid solutions in the past few years, it is important to point out that the commercial sales of PICs continues to be dominated by InP-based solutions. Fig. 1 gives a bar chart of the sales of optical transceivers in the recent past along with projections for the next five years at this writing (2017)

Manuscript received May 8, 2017; revised June 30, 2017; accepted September 15, 2017. Date of publication September 20, 2017; date of current version October 6, 2017. This work was supported in part by DARPA-MTO under the DODOS Project and in part by the National Science Foundation under Grant 1402935. *(Corresponding author: Shamsul Arafin.)*

The authors are with the Department of Electrical and Computer Engineering, University of California, Santa Barbara, CA 93106 USA (e-mail: sarafin@ucsb.edu; coldren@ucsb.edu).

Color versions of one or more of the figures in this paper are available online at http://ieeexplore.ieee.org.

Digital Object Identifier 10.1109/JSTQE.2017.2754583

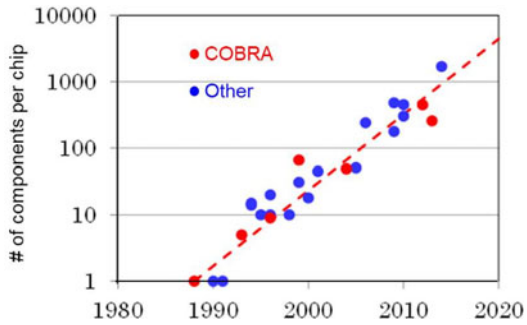


Fig. 2. Evolution of chip complexity measured as the number of components per chip over time. Figure was based on the data from [18].

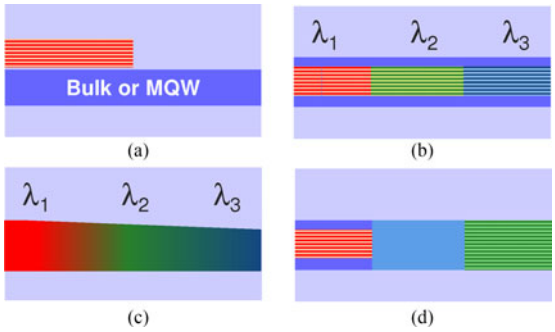


Fig. 3. Several active-passive waveguide integration approaches, (a) offset-quantum wells, (b) QW intermixing, (c) selective area growth, and (d) butt-joint regrowth. Courtesy: Lumentum.

[14]. Such transceivers dominate the optical component market. There is an additional ∼$1 B in sales over this time period for optical amplifiers and passives that is relatively flat. As can be observed, InP PICs currently provide the largest sales component, and they are projected to continue to be the dominant component, perhaps for the next decade or so. This is why the current and future research on InP-PICs is justified.

There have been a few excellent and comprehensive reviews on InP-based PICs and its generic integration technology recently published [15]–[19]. In this paper, we have chosen to focus on the more recent advances on InP-PICs, being suitable for coherent communication and sensing applications, which have not been covered in the prior reviews.

Nevertheless, it is worthwhile including a chart from [18] that indicates the growth in the number of components per chip over time, and this is shown as Fig. 2. It shows the complexity development over forty years. Interestingly, there are other charts for optical communication PICs that show plots of data capacity per chip in Gbps which also have nearly the very same trend line [20]. So, the title could just as well be "Data Capacity/Chip (Gbps)".

To get started with the body of this paper, we first will briefly review the current thinking on active-passive waveguide integration techniques, critical for active PICs, in Section II. There continue to be a number of choices, but there appears to be some agreement on the tradeoffs. Then in Section III, a brief sampling of recent commercial PIC advances gives an example of the status of a decades-old PIC design as well as much more complex and highly functional PICs available today; then moving on to Section IV where a review of analog functionalities gives examples of recent programmable filters and signal processing elements not discussed in prior reviews. Section V, entitled sensing by beam sweeping and light detection and ranging (LiDAR), introduces a novel coherent transceiver PIC, and gives a summary of prior results from some of its elements; finally in Section VI, optical phase-locked loops (OPLL) for low-cost/power coherent receivers and synthesis, the advantages of the close integration of coherent receiver PICs with feedback electronics is explored in a couple of applications.

## II. Recent Thinking on Active-Passive Integration

Prior to discussing the various advanced InP-PICs, recently developed by industry and academia, it is important to provide a short overview of the integration technology platforms that they have used. It is desirable for these platforms to enable the monolithic integration of different active and passive components with a minimal compromise in the performance of the individual components. As illustrated in Fig. 3, several commonly used integration platforms include offset quantum wells, quantum well intermixing (QWI), selective area growth, and butt-joint regrowth [2]. Among these platforms, the butt-joint regrowth technique is most popular with the more established industries due to its ultimate design flexibility [17]. Since the multiple active and passive waveguide structures are created in different growth steps, a large flexibility in the material composition, number and width of quantum wells and doping can be provided in each section. However, this benefit comes with additional growth steps. For a complex PIC, it could require five or more regrowths to achieve the desired multiple bandgaps, perhaps resulting low yield in the devices, if extreme precision is not available.

Offset quantum well (OQW) and quantum well intermixing (QWI) are other two integration platforms which tend to be more widely used in academic research and industries where the availability of epitaxial growth equipment is not available, or where regrowth technology is not well developed. In both cases, an unpatterned cladding regrowth [2] is performed with only a small or negligible height change between the active and passive regions, and this regrowth can usually be performed by commercial vendors. One of the disadvantages of this technique is that the doping concentrations in the active and the passive cladding layers are the same, introducing higher absorption losses in the transparent regions.

Multiple bandgaps are possible in the QWI process by multiple etching and annealing steps, but the in OQW case, double (again planar) regrowths are generally necessary for three bandgaps. QWI has also been used at surfaces to increase the bandgap of active regions and thus make transparent regions that might otherwise be absorbing because of surface recombination inhibiting carrier build-up to a transparency level. Especially in Al-containing materials of high-power lasers, facet damage is a well-known consequence [21]–[22], and this can also show up as unwanted 'active' absorption loss in other structures.

The final integration platform, selective area growth (SAG), is used commercially in electroabsorption modulator

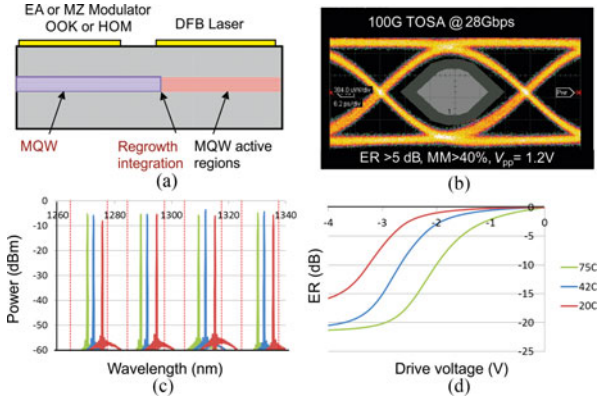


Fig. 4. (a) DFB laser with an integrated modulator for optical transceivers in metro or datacenters, (b) eye diagram measured at $V_{pp} = 1.2$ V; ER $> 5$ dB, (c) optical spectra-100 gigabit ethernet (GbE) CWDM4, and (d) transfer function of EAM optimized for uncooled applications. Courtesy: Lumentum.

(EAM)/distributed feedback (DFB)-laser PICs [23], and is particularly interesting because multiple-bandgap devices can be grown in a single step by just changing the width of dielectric-coated regions beside the waveguide regions-to-be during the initial epitaxial growth. Because precursors will not decompose and grow on the substrate over the coated regions, they 'pile-up,' diffuse laterally, and provide for a thicker growth beside the coated regions. The width of the coated regions determines the amount of the increase in thickness, and for QWs, the reduction in effective bandgap. For quaternary growth on InP, there are limitations on the compositional range over which this can be accomplished, due the need to approximately lattice match.

This technique is also currently being used in combination with butt-joint regrowth in some commercial devices. This allows some regrowth steps to be eliminated, where the doping levels can be the same in some adjacent regions [24].

## III. Sampling of Recent Commercial InP-PIC Advances

This section will focus on a short overview of several different types of InP-PICs by commercial vendors, which will show the recent advances, PIC complexity and technological maturity. In addition to these commercial PICs, there have been also a quite bit of successful academic or foundry works recently reported in this area [25]–[27].

Fig. 4(a) illustrates a recent state-of-the-art example of one of the oldest PIC concepts, which dates back to the mid-1980's [28], [29]. This is a simple DFB laser with EAM integrated on a single chip of InP. The integration avoids any chip-to-chip coupling optics with associated losses, expense, and reliability issues, and the bandgap of the modulator is adjusted to be appropriately offset from the wavelength of the laser during fabrication [30], [31]. With proper design, the device can operate over a wide temperature range by only offsetting the DC bias voltage. Applications are for datacom, perhaps in data centers.

The commercial vendor, Lumentum successfully demonstrated such InP-based PICs and its eye diagrams were measured at 28 Gbps for a transmitter optical subassembly (TOSA) calibrated at 0 dBm time averaged output power per channel, as presented in Fig. 4(b). This is a major step forward

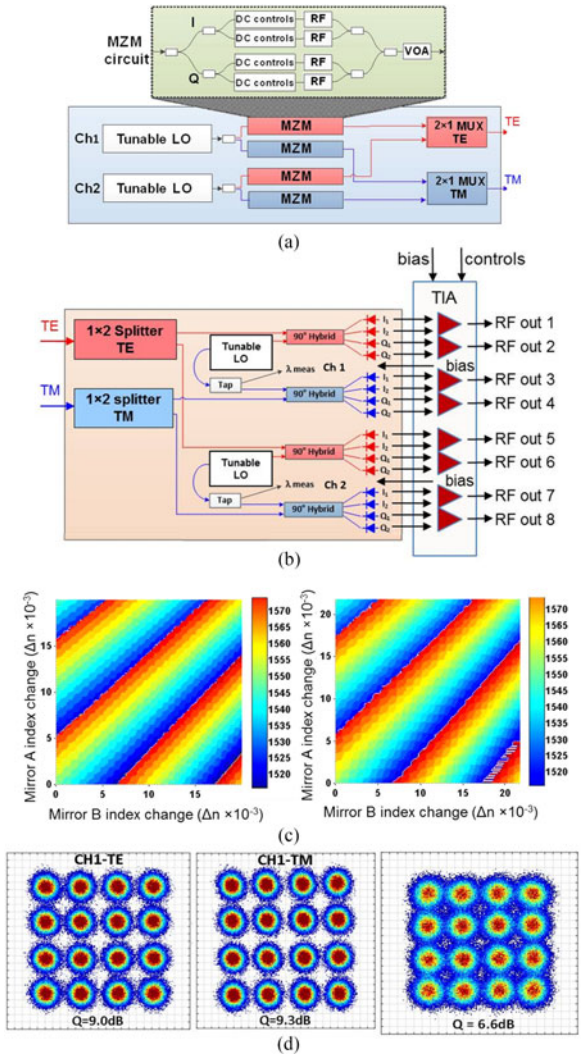


Fig. 5. (a) 2-Channel Tx PIC architecture, (b) 2-Channel Rx PIC and TIA ASIC architecture, (c) laser tuning maps of Tx. Each map shows the laser output wavelength as a function of the estimated effective index change on the two mirror sections, and (d) recovered constellations at 88 Gbd $\times$ 16 QAM from a reference Tx, EDFA, 80 km fiber and Rx PIC wire-bonded to a TIA receiver (left); 88 GBaud 16 QAM constellation after propagation over 80 km of SMF from a Tx PIC to a Rx PIC wire-bonded to a TIA receiver (right). Courtesy: Infinera.

in terms of low requirements on the drive voltage, ensuring compatibility with low power dissipation modulator drivers and improving the power budget of the transceivers. The spectral characteristics of electroabsorption modulated laser (EML) based $4\lambda \times 25$ Gbps coarse wavelength division multiplexing (CWDM)-TOSA are presented in Fig. 4(c). Fig. 4(d) shows the typical transfer function of the EAM optimized for uncooled applications. The slope of the transfer function exceeded 10 dB/V, providing high modulation efficiency with low insertion loss.

Fig. 5 shows recent results from Infinera's multi-channel widely-tunable coherent transmitter (Tx) and receiver (Rx) PICs, which together form a flexible high-capacity link. With 2 Channels $>$ 700 Gb/s per channel (via 88 Gbaud, 16-QAM dual-polarization modulation) over 80 km was demonstrated. That is, a total capacity of 1.4 Tbps could be available using

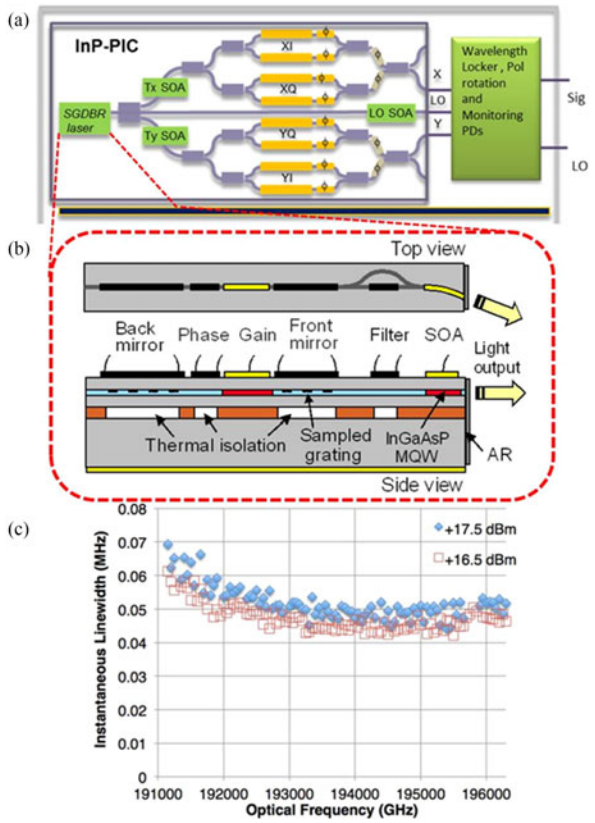


Fig. 6. (a) Schematic layout of monolithic InP-PIC consisting of thermally tuned narrow linewidth C-band tunable SG-DBR laser, dual-polarization *I-Q* modulators, and three SOAs, (b) schematic of a monolithic widely-tunable SGDBR laser utilizing high-efficiency thermal index tuning design, and (c) linewidth as a function of optical frequency. Courtesy: Lumentum.

both channels. Tuning across the entire C-band in both the Tx and Rx insures arbitrary wavelength reconfigurability [20], [32].

Both Tx and Rx chips have a two channel design. The Tx chip incorporates two independent widely-tunable lasers, each split into two nested Mach-Zehnder modulators (MZM) for *I-Q* modulation of a TE and TM-to-be channel. Each MZM can run up to 88 Gbaud with various modulation formats. The two TE or TM channels are combined at the output of the chip.

The Rx chip has TE and TM inputs, each of which are split into two channels. The outputs of two widely-tunable LO lasers are each divided in two and one half combined with a TE and the other a TM output from the two splitters by a 90° hybrid. The four outputs (*I, I', Q*, and *Q'*) of the four 90° hybrids become the four sets of outputs to the electronics for the TE and TM channel modes of the two channels.

Infinera plans to incorporate modules with these PICs within their future optical communication systems, as with their other PIC-based systems. That is, the Rx and Tx modules containing the PICs described in Fig. 5 will not be externally available as standalone products.

Fig. 6 illustrates Lumentum's single-channel widely-tunable Tx PIC, configured for advanced modulation format TE and TM transmission, which also provides an output for the LO of a co-located Rx [33]. Of particular interest is the widely tunable laser, which has very desirable output characteristics.

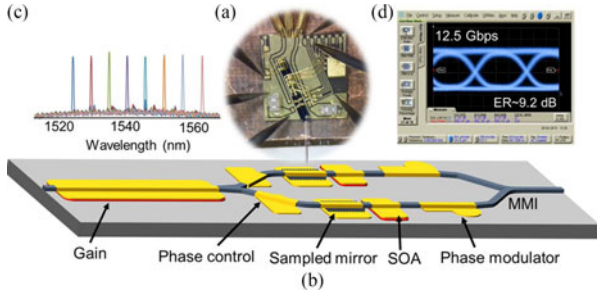


Fig. 7. (a) Microscope image of InP-PIC as a tunable interferometric transmitter mounted on the AlN carrier and wirebonded, (b) schematic layout of such a PIC with integrated traveling-wave modulators, (c) optical spectra of the on-chip SG-DBR laser lasing at different mirror super-modes, and (d) eye diagram measurements of the PIC for 12.5 Gbps operations. Courtesy: Freedom photonics.

The output power exceeds 50 mW; the linewidth is less than 70 kHz; and the side-mode suppression ratio is greater than 50 dB across the entire C-band. No other integrated widely-tunable laser competes with these characteristics. The nested MZM is similar in design to that described above following Fig. 5. Also of note is that Lumentum makes available such widely-tunable Tx modules of this design [33], [34].

In addition to a high-performance InP-PIC-based transmitter, demonstrated by Freedom Photonics Inc. [35], a new and novel form of widely-tunable transmitter is recently reported [36]. This transmitter, shown in Fig. 7, is based on a type of dual-output Y-branch laser, a pair of high-speed phase modulators, and a multimode-interference (MMI) coupler to complete a MZM at what would have been the dual output side of the laser [36]. Compared to the existing technology, such a compact and cost-effective transmitter achieves the functionality of an integrated widely-tunable laser with a MZM, a so called integrated laser Mach-Zehnder (ILMZ), to provide controllable chirp outputs, etc., but much more elegantly. By only adding a phase modulator at the end of each Y-branch laser output arm followed by the combining MMI, the ILMZ is complete.

Fig. 7 shows a photo of a mounted device, a device schematic, superimposed spectrum, and an eye diagram. A tuning range of 50 nm was observed; The SMSR was 50 dB; the eye was taken at 12.5 Gbps with an extinction ratio of $>$ 9 dB; over 80 km reach observed in standard SMF-28 fiber. The phase modulators used in this work used a bulk electro-optic effect. Improved responses are expected with quantum well designs.

Fig. 8 illustrates the ability to integrate multiple widely-tunable transmitters and combined into a single output on a single chip. These were SGDBR lasers followed by SOAs and EAMs, and then finally combined in a $4 \times 1$ wide-band power combiner. The PIC operates well at 55 °C for reduced TEC power. SOAs enable variable optical attenuator (VOA) and blanking functions for high-speed switching between lasers. Eye diagrams illustrate full functionality of the PIC.

## IV. Analog Functionalities

In RF-photonic and analog fiber optic links and systems, two key components, a linear optical modulator and a tunable

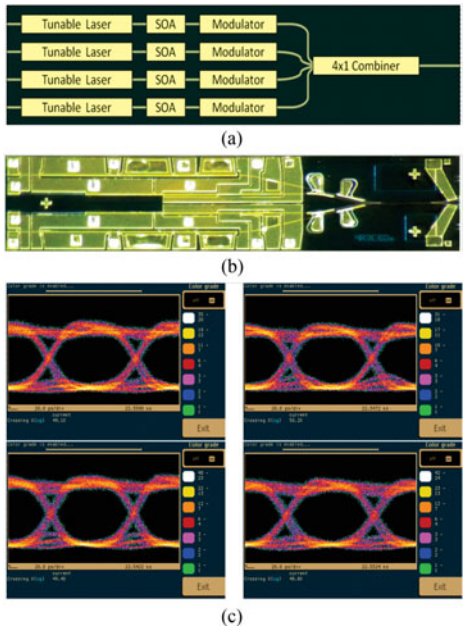


Fig. 8. (a) Schematic layout of a quad-transmitter using InP-PICs, (b) microscope image of the monolithic InP C-band tunable transmitter with single output waveguide, and (c) eye diagram measurements of the all transmitters. Courtesy: Freedom Photonics.

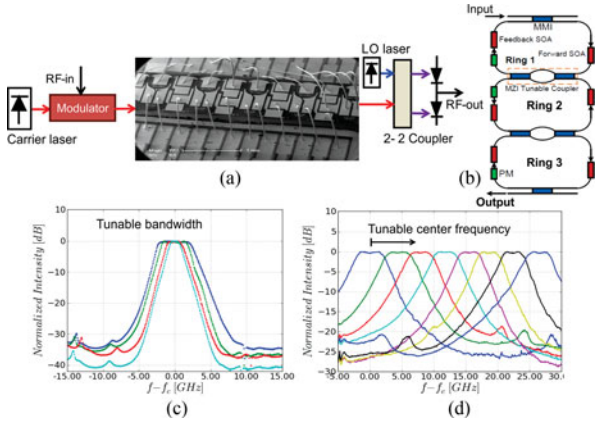


Fig. 9. (a) Test set-up for PIC filter, and balanced receiver. The optical signal is in red, RF electrical signals in black, and LO in blue, (b) schematic representation of third-order coupled-ring filter. MMIs are in blue, SOAs in red, and phase modulators (PMs) in green, (c) 3rd order tunable bandwidth result, and (d) center frequency tunability demonstrated using a 2nd order bandpass filter. Reproduced with permission from [40].

optical filter can be important for reducing the signal distortion and achieving a high dynamic range. Linear modulation of RF directly onto the optical wave is desired in a number of applications. Analog RF-photonic links for antenna remoting is one example. In this case, optical fibers can replace microwave cables between the equipment bay and the antenna, perhaps on ships or airplanes, where size, weight and transmission loss are important. Key criteria are overall link loss, noise figure, bandwidth, and dynamic range. To meet these criteria, ring-assisted MZI (RAMZI) modulators, proposed in 2003 [37], have been used in InP- PICs [38], [39].

In an analog RF-photonic system, an optical tunable filter is also highly desirable as the second key component. It is often desired to incorporate optical filters to isolate flexible communication channels or weaker portions of the optical spectrum near stronger ones received for more detailed analysis. Fig. 9 outlines results from a multi-section active ring-resonator filter PIC formed on InP.

For testing, a coherent heterodyne RF photonic link is formed as shown in Fig. 9(a). In such a system, a photonic carrier signal is phase modulated using the RF input. The modulated carrier signal goes through the InP-PIC filter to be evaluated. A strong local oscillator (LO) laser down-converts the InP-PIC-filtered optical signal through a balanced detection receiver.

Tunable bandwidth and tunable center frequency RF photonic filters were developed by Norberg *et al.* [40] and Guzzon *et al.* [41]. Cascaded and coupled-ring bandpass filters were fabricated and demonstrated in this study, showing high levels of tunability and near-ideal filter shapes. Fig. 9(b) shows a schematic of a third-order coupled-ring bandpass filter. The tunable coupling between two neighboring rings and between the outer ring and the bypass waveguide was realized using four tunable couplers each consisting of two multimode interference couplers and two PMs. Fig. 9(c) gives results of bandwidth adjustment, and Fig. 9(d) shows the tuning of the center frequency in a two-section coupled-ring configuration.

The optimal Spur-free Dynamic Range (SFDR) and Noise Figure (NF) was obtained with the SOA gains adjusted such that the overall filters had near zero net insertion loss. SOAs were designed with separation layers between the waveguides and active regions to increase their saturation levels to ∼19 dBm. In this case, the NF and SFDR were measured to be ∼4 dB and ∼115 dB-Hz$^{2/3}$, respectively. These are very good numbers, and quite unexpected with SOAs included within the filters, but it turns out that removing the insertion loss is more important than the ASE added by the SOAs.

In today's optical communication links, signal processing is still performed digitally using electrical systems. This standard digital signal processing requires electronic sampling, optical-to-electrical and electrical-to-optical conversions to reconstruct the signal in the receiver side. This is mainly due to the fact that digital signal processing in the electrical domain suffers from the limited speed due to much lower electronic sampling rate. By contrast, equivalent signal processing in the optical domain offers the advantages of relieving the inherent time-bandwidth constraints in electrical systems. Therefore, implementing signal processing directly in the optical domain in these optical links will eliminate the necessity of electronic sampling, OE and EO conversions, paving the way for achieving power-efficient and high-speed signal processing [42].

Considering this, Liu *et al.* [43] used the same integrated multi-section active ring filters described in Fig. 9 above to perform reconfigurable signal processing functions, including temporal integration, temporal differentiations and Hilbert transformation. Fig. 10(a) shows a fabricated InP-PIC used in this study. Two active microring resonators and a bypass waveguide, as schematically shown in Fig. 10(b), were utilized. To obtain on-chip reconfigurability, six semiconductor optical amplifiers (SOAs) and five current-injection phase modulators (PMs) in

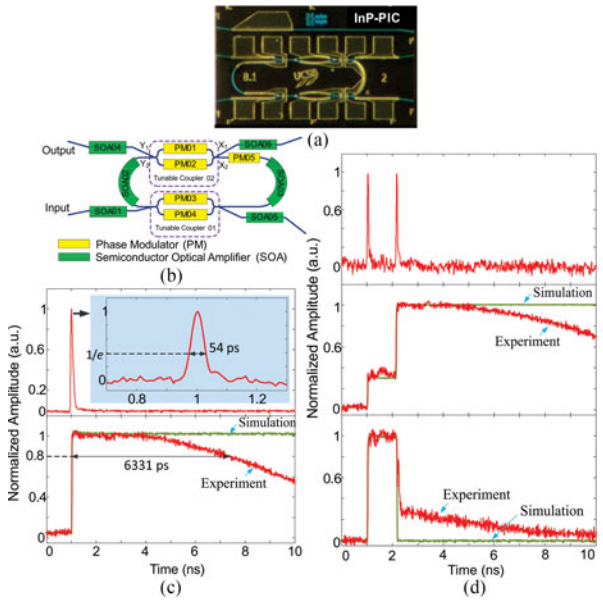


Fig. 10. (a) Microscope image of the processed on-chip photonic temporal integrator prototype based on InP-PICs, (b) its schematic illustration, (c) the experimental results, where the input Gaussian pulse with a temporal width of 54 ps (top); the integral of the Gaussian pulse with an integration time window of 6331 ps (bottom), and (d) the input in-phase doublet pulse (top); the integral of the in-phase doublet pulse (middle); the integral of the out-of-phase doublet pulse (bottom). Reproduced with permission from [43].

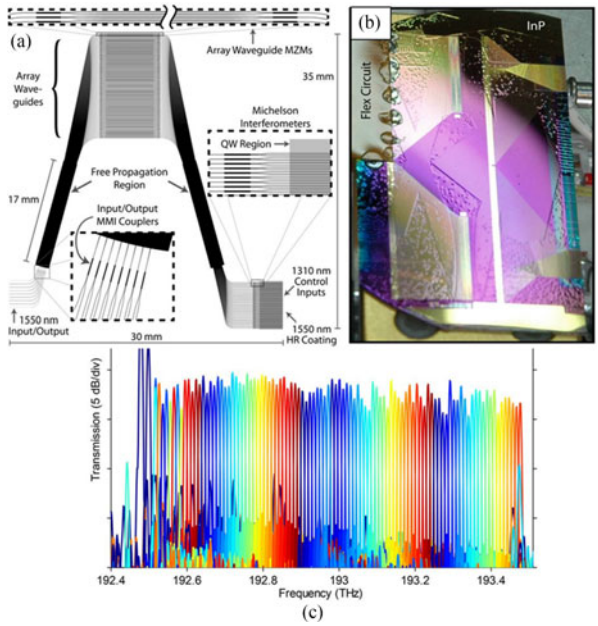


Fig. 11. (a) Mask layout of a single 100-channel × 10-GHz OAWG device, (b) two fabricated InP devices from a single 2-inch wafer with a flex circuit attached to one device, and (c) single-pass 100-channelx 10-GHz AWG output spectrum after phase-error correction. Reproduced with permission from [45].

the unit cell [43] were used. In this way, a photonic temporal integrator with ultra-high power efficiency and a continuously tunable operating wavelength was achieved.

The authors tested the operation of such an InP-PIC based signal processor that was configured as a photonic temporal integrator. By configuring the photonic temporal integrator with the injection currents to the SOAs and PMs in the ring, a high Q-factor of $31 \times 10^6$ was achieved and the ring was still under the lasing threshold. As shown in Fig. 10(c), the temporal integral of the input Gaussian pulse is realized. The presented photonic integrator provided a time-bandwidth product of $\sim$100, which is far better than an advanced electronic integrator.

The authors also tested the integration of an in-phase doublet pulse by the proposed photonic temporal integrator. In Fig. 10(d), the integrator sums up the area of the in-phase doublet, giving two steps corresponding the area of the first pulse and the area of the first and the second pulses. With a $\pi$-phase shift (out-of-phase), a memory resetting function is performed by the integrator.

In addition to the use of InP-PIC based optical filters and reconfigurable signal processors in analog RF-photonic systems, other types of PICs show a number of analog functionalities, including optical arbitrary waveform generation (OAWG) [44]. Such analog PICs for OAWG have found applications in areas of optical communications and arbitrary optical/RF waveform generation. In late 2011, a monolithically integrated OAWG based on InP-PICs with access to 1 THz of optical bandwidth was demonstrated [45].

In this study, the authors demonstrated an optical waveform shaper that can manipulate the amplitude and phase of a stable optical frequency comb (OFC) on a line-by-line basis. These InP-based OAWG devices consisted of a 100-channel arrayed-waveguide grating (AWG) spaced at 10 GHz with 100 Michelson interferometers, 200 QW phase modulators and 400 electro-optic MZMs in twin configurations on a single 2 inch wafer.

The mask layout of OAWG devices with an overall dimension of $3\,\mathrm{cm} \times 3.5\,\mathrm{cm}$ is shown in Fig. 11(a). Two fully-processed devices are shown in Fig. 11(b) where the upper device was a mirror image of the lower one. Devices with a cleaved-facet at the left side used a $2 \times 1$ MMI coupler as the 1550-nm input and output. The input/output side is zoomed-in and the detail of each MMI coupler is shown in the inset. The AWG contained 400 arrayed waveguides and, each had an electro-optic MZM. Each of the 100 AWG outputs had a Michelson interferometer consisting of a $2 \times 1$ MMI splitter/combiner, as shown in the inset of Fig. 11(a). The interferometer arms had a 1-mm-long QW phase modulator and an HR/AR-coated cleaved-facet mirror with a reflectivity of 86% at 1550 nm and 6% at 1310 nm.

The successful operation of OAWG devices requires high adjacent channel isolation resulting low crosstalk for the MUX and overlapping passbands for the DEMUX. Fig. 11(c) shows the measured single-pass AWG transmission for all 100 AWG outputs after phase-error correction (TE polarization). The data were taken by moving a fiber to each AWG output channel and making a measurement with the Optical Vector Network Analyzer. Each output was recorded and the average channel bandwidth of 6 GHz was reported. The average calculated crosstalk values were measured to be 15.1 dB. This represents one of the largest area InP-PICs ever fabricated.

Despite of the academic proof-of-principle, it is an open question whether such a very large InP-PIC based AWG can be

mass-fabricated, even in more mature foundry technologies, due the large number of long waveguides.

## V. Sensing by Beam Sweeping and LiDAR

Optical beam generation, shaping and steering based on optical-phased array (OPA) technology are currently of significant research interests due to lots of emerging applications, including free-space optical communication, 3D imaging and mapping in LiDAR systems and autonomous cars [46]. Over the last couple of years, considerable research effort has been made for the development of highly-integrated and reduced size, weight and power consumption beam steering systems utilizing PICs. Several beam steering demonstrations based on PICs using either InP- [47]–[49] or silicon platforms [50] are already reported.

Recently, Guo *et al.* demonstrated 2-D optical beam steering with an InP-PIC using the scheme of 1-D OPA plus wavelength tuning with surface-emitting gratings [47]–[49]. In this case, the 1-D OPA scans the beam laterally, while axial scanning is achieved by varying the wavelength of a widely-tunable laser via the surface-emitting grating. An InP platform was chosen because all of the active and passive components necessary for the desired rapid 2-D beam steering could be integrated on a single PIC. This includes the rapidly-reconfigurable and widely-tunable laser for axial scanning, the high-power SOAs for sufficient power to all waveguide elements of the OPA, and efficient and rapidly-tunable phase shifters for each waveguide of the OPA. In this case, a SGDBR laser was chosen and forward-biased current-injection phase-shifters were selected.

Fig. 12(a) shows the layout of the SWEEPER-PIC. It utilized 32-element OPA. The free-space splitter was fed by either an SGDBR with ∼45 nm of wavelength tuning or an external laser input. The free-space splitter excited 32 waveguides that flared out over a width of ∼3.5 mm to spread the heat from the following phase-shifters and SOAs. Each waveguide had a separately contacted phase-shifter and SOA. The waveguides were then brought back together in a non-uniformly spaced array to suppress sidelobes, as shown in Fig. 12(b).

The grating region was covered with a metal layer spaced by effectively one wavelength above the waveguide in the medium to enhance the bottom emission, and this was slightly off of normal to avoid back reflections. Fig. 12(c) shows intensity scans of the one-dimensional (1D) far-field both longitudinally (axially) and laterally, whereas Fig. 12(d) presents 3D plots of the optimized far-field patterns. There was an on-chip monitor array for each channel after grating. The PIC contained 104 diodes in total. Beam steering angle range of 6° in the longitudinal direction and 12° in the lateral direction were reported with the on-chip laser. Wider longitudinal sweeping was possible with an off-chip laser.

More recently, there have been some ongoing research efforts to demonstrate a LiDAR system based upon the SWEEPER concept. For this, a more complex InP transceiver PIC is being explored as well as its integration with a Si-photonics emitter PIC. Fig. 13(a) illustrates the concept [51]. In this case, the InP-PIC transceiver is flip-chip bonded to the Si-photonics

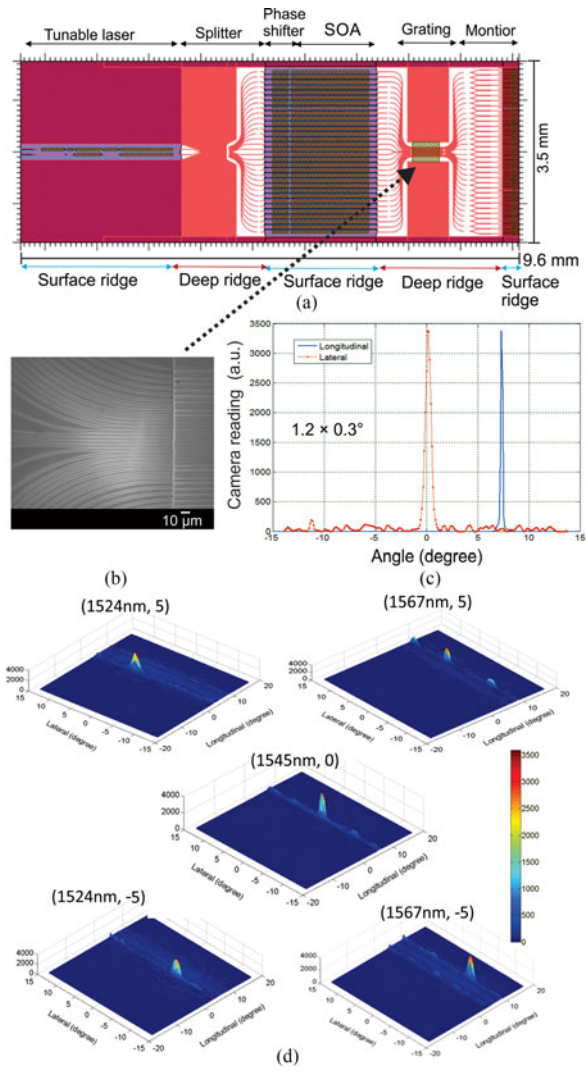


Fig. 12. (a) Schematic and (b) mask layout of the InP-PIC for 32 × N surface emitting grating phase array, and (b) SEM images of waveguide feeds from splitter and into grating arrays, (c) one-dimensional, and (d) three-dimensional plot of the far-field patterns for some critical angles in the longitudinal and lateral directions, wavelength controlling the longitudinal direction and phase shifters controlling the lateral direction. Reproduced with permission from [49].

(SOI)-PIC, and light is coupled to a waveguide on the SOI, where the optical splitter, phase-shifter (modulator) array and 1-D grating surface-emitting waveguide array (OPA) exists. Electrical contacts to the InP-PIC are also made to the SOI-PIC. The SOI in turn, is flip-chipped to a Si-interposer which contains the drive and control electronics for both the InP-PIC transceiver and the SOI-phase modulators. The InP-PIC transceiver, illustrated more explicitly in Fig. 13(b), contains an asymmetric MZ (AMZ) filter and detectors for a wavelength locker as well as couplers and detectors for a coherent receiver in addition to the widely-tunable SGDBR laser. With the addition of external feedback electronics from the AMZ filter detectors to the phase tuning section of the laser, the locker selects and stabilizes the laser to specific wavelengths across its widely-tunable spectrum. These wavelengths correspond to directions in the far-field for the resulting optical beam. Also, thermal transients can be eliminated following a wavelength tuning event. Finally, the AMZ

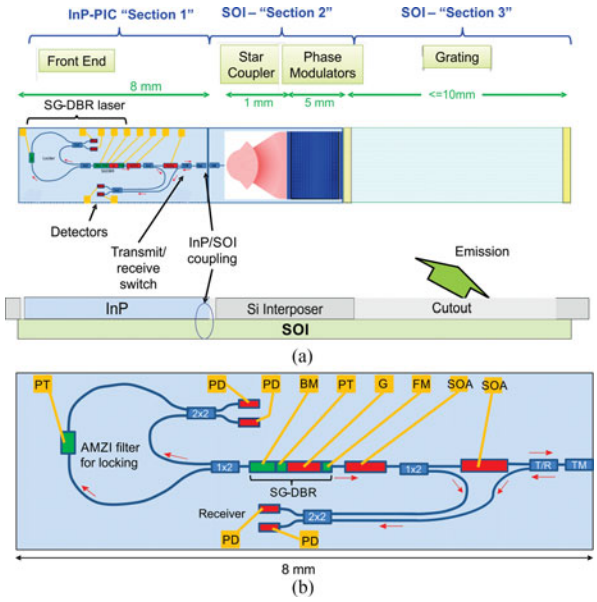


Fig. 13. (a) Hybrid integration of InP-transceiver PIC with a SOI-emitter PIC on a Si-Interposer, and (b) schematic layout of the InP-PIC. (BM = back mirror, FM = front mirror, G = gain, PD = photodiode, PT = phase tuner, SOA = semiconductor optical amplifier, TM = turning mirror, T/R = transmit/receive.)

filter is also tunable by the addition of a phase shifter in one of its arms—upper left-most contact pad in Fig. 13(b). This provides for a possible continuous ramping of the output frequency of the laser while it is locked, enabling an frequency modulated continuous wave (FMCW) type of LiDAR to be implemented [51].

The coherent receiver is formed by coupling a portion of the SGDBR's output to the receiver coupler as the LO, where it is combined with a portion of the return echo from the SOI emitter/receiver stage. For the FMCW case, these waves mix in the two receiver photodiodes to provide the heterodyne current to the external receiver electronics. The frequency of the return wave is slightly different from the present SGDBR value, because of the delay and the frequency sweep rate of the laser. For example, if the laser were to be swept at a rate of 100 MHz/$\mu$s and the delay of the return echo was 1 $\mu$s, then the heterodyne difference frequency would be 100 MHz, and this would then determine the distance to the object causing the echo.

The viability of the coherent LiDAR PIC of Fig. 13 is supported by the fact that some of its key elements have already been successfully demonstrated. For example, the very important wavelength locker, which both stabilizes the wavelength output and enables wavelength chirping, has been demonstrated before using InP-PICs. As shown in Fig. 14, AMZI filters have been integrated with SGDBRs, and with feedback electronics shown vast improvements in wavelength stability [52], [53]. In fact, this prior work shows the same design as incorporated within Fig. 13. The InP-PIC consists of a widely-tunable SG-DBR laser, a 60 GHz free spectral range (FSR) AMZI, and waveguide detectors monolithically integrated on the InP platform. A microscope image of the PIC can be seen in Fig. 14(b) together with a circuit schematic. The basic idea of such wavelength locking is that the optical frequencies of the

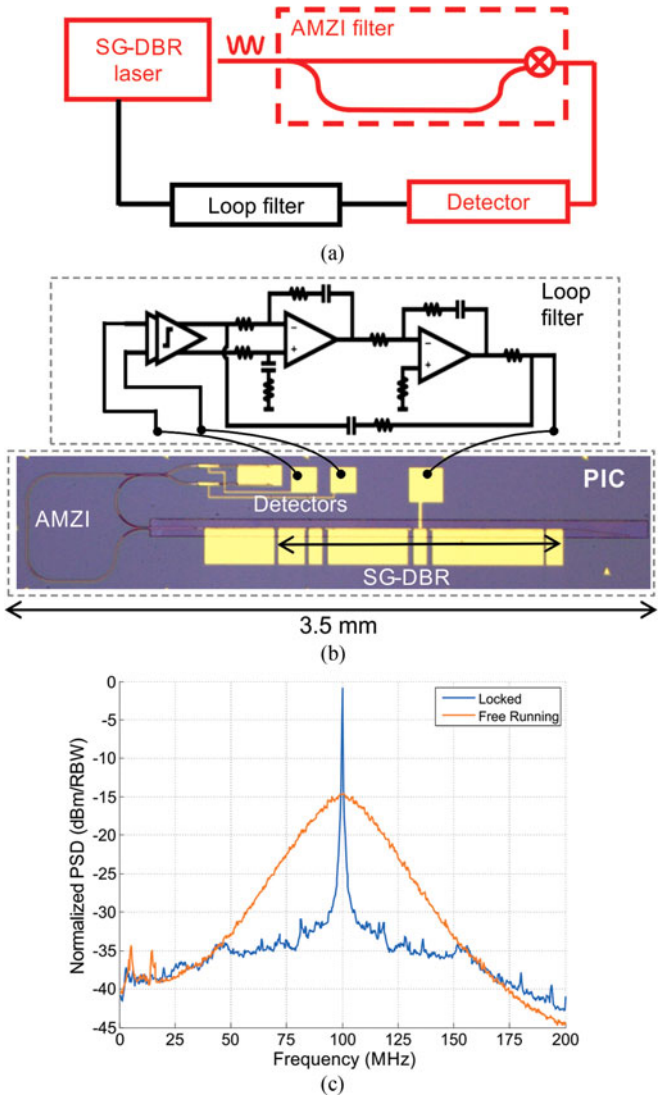


Fig. 14. (a) Schematic of the frequency lock loop system using an InP-PIC, (b) micrograph of the InP-PIC with a schematic of the feedback electronics including loop filter and (c) ESA spectra of the free running and locked SGDBR laser. The 3-dB linewidth after locking is 150 kHz. Reproduced with permission from [52].

SG-DBR laser can be stabilized by locking at the zero-crossings of the on-chip AMZI filter. The high-gain of the feedback loop provides an error signal to the laser tuning phase section that forces the wavelength to shift until there is essentially no input current to the circuit. If the gain is sufficiently high even frequency noise that would cause a natural dithering about this operating point is significantly suppressed. This latter effect is shown in Fig. 14(c), where the linewidth is reduced from an initial value of several MHz down to 150 kHz with frequency locking.

Another building block in the LiDAR system of Fig. 13 is the efficient coupling of light from the InP transceiver PIC to-and-from the SOI emitter PIC [54]–[56]. With flip-chip bonding, vertical coupling is required. A technique, employing a grating coupler on the SOI waveguide and a TIR reflector within the InP-PIC, has been recently explored [57]. Fig. 15(a) illustrates

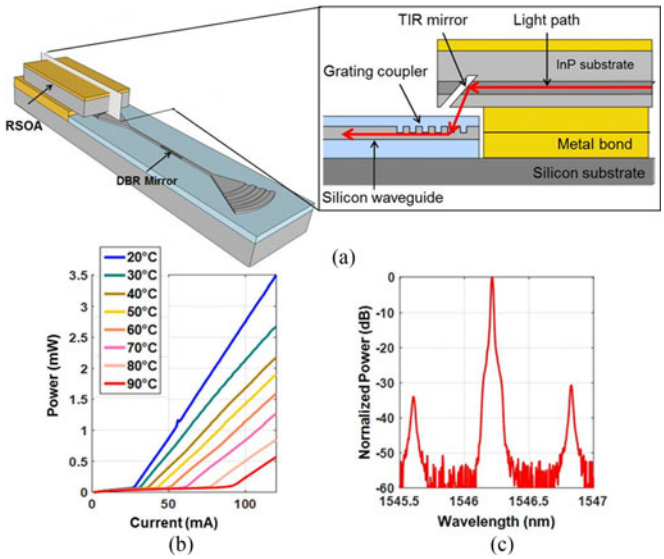


Fig. 15. (a) 3D schematic of the InP-PIC bonded to the silicon substrate for, 3D integrated hybrid silicon laser, and a cross-sectional schematic is zoomed-in, illustrating vertical coupling using turning mirror, (b) temperature dependent *LIV* curves and (c) lasing spectrum of the of the hybrid laser. Reproduced with permission from [56].

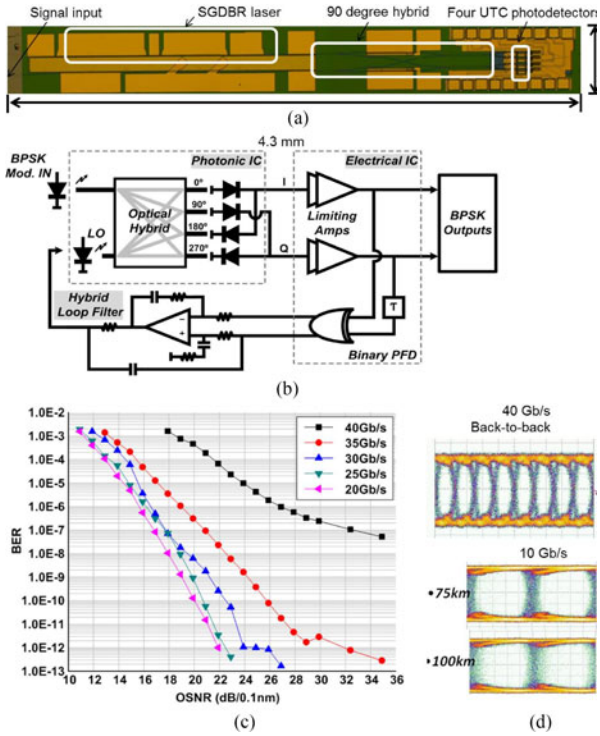


Fig. 16. (a) Microscope image of the InP-PIC used for developing OPLL systems, (b) schematic of the Costas loop based phase-locked coherent BPSK receiver using this PIC, (c) bit error rate (BER) vs optical signal-to-noise ratio (OSNR) curves of the receiver, measured at the data rates from 20–40 Gbps, and (d) eye diagrams of received data at 40 Gbps for a back-to-back experiment as well as at 10 Gbps after 75 and 100 km fiber propagation. Reproduced with permission from [58].

this technique schematically. As a matter of fact, this approach is based on the flip-chip integration of InP-PICs containing total internal reflection (TIR) turning mirrors for surface emission. In refs. [54]–[57], light was coupled to the SOI waveguides through surface grating couplers, as shown in Fig. 15(a). Fig. 15(b) shows the temperature dependent continuous-wave *LIV* characteristics. The maximum operating temperature of these devices was 90°C. Devices showed reasonably good wall-plug efficiency due to an excellent heat management. Fig. 15(c) show the lasing spectra of the hybrid laser at a bias current of 60 mA, measured at room temperature. Devices exhibit single-mode operation with a side-mode suppression ratio (SMSR) of 30 dB or greater.

## VI. OPLL for Coherent Receivers and Frequency Synthesis

Although coherent communication in today's optical links is being used, it is mainly based on the high speed analog-to-digital converter (ADC) and digital signal processor (DSP) to recover the phase information, which makes the receiver power-hungry and less cost-effective. Therefore, it is currently of significant interest to develop compact, efficient and cost-effective analog coherent optical receivers that do not require ADC or DSP. In 2012, a highly-integrated 'analog coherent' optical receiver using InP-PICs was achieved [58], [59]. A homodyne optical phase-locked loop (OPLL) technique with a Costas loop was employed in such a receiver. A photonic IC, an electrical IC, and a hybrid loop filter were developed to build a stable homodyne OPLL. Finally, the binary phase-shift keying (BPSK) receiver based on Costas loop exhibited error-free ($\mathrm{BER} < 10^{-12}$) up to 35 Gbps with no latency. The integrated Costas receiver has its advantage in better phase noise suppression, high BER, small footprint, power efficiency and cost-effectiveness.

The fully-processed PIC based on the InGaAsP/InP platform used in this study is shown in Fig. 16(a). The PIC included a widely tunable SG-DBR laser with a 40 nm wavelength span by current injection into front and back mirrors and a phase-tuning section diode. The received signal from the reference laser and LO laser were mixed by an integrated 90° optical hybrid and down-converted by four uni-traveling carrier PDs for *I-Q* electrical outputs. The fabricated optical hybrid had $\pm$ 2% imbalanced outputs and the PDs exhibited a 3-dB bandwidth of 30 GHz and 18 mA saturation current at $-5$ V.

The general architecture of the optical Costas loop-based analog coherent optical receiver is shown in Fig. 16(b). The *I-Q* signals were detected by four high speed photodetectors, which not only converted the optical signal to electrical signal, they also acted as low pass filters. The mixer was realized by a delay line and an XOR gate, which act together as a quadri-correlator phase/frequency detector (PFD). The error signal from the PFD fed back to the laser tuning section through the loop filter.

The authors measured the bit-error-rate (BER) and eye diagrams of the received BPSK data. The BER measurement was carried out at the bit rates of 20, 25, 30, 35, and 40 Gbps. By varying the VOA, the optical signal-to-noise ratio (OSNR) from the EDFA output changes, and therefore the BERs are measured at different OSNR. The results are shown in Fig. 16(c). The measured eye diagrams at 40 Gbps for the back-to-back experiment are shown in Fig. 16(d), from which we can see the eyes are

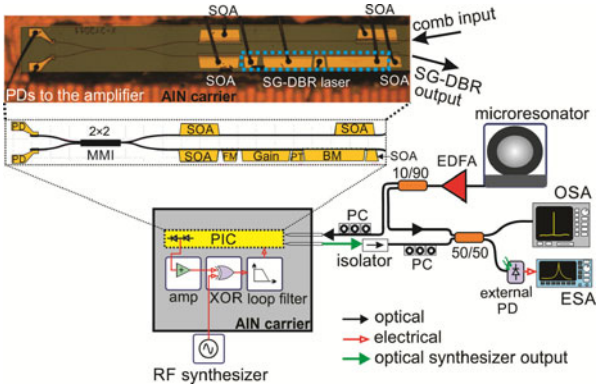


Fig. 17. The test setup of the optical synthesizer using heterodyne OPLL locking scheme. A microscope picture of the fully fabricated PIC mounted on AlN carrier with wirebonding shown at the top. (amp: amplifier, BM: back mirror, ESA: electrical spectrum analyzer, EDFA: erbium doped fiber amplifier, FM: front mirror, MMI: multimode interference, OSA: optical spectrum analyzer, PC: polarization controller, PT: phase tuner, PD: photodetector, PIC: photonic integrated circuit, SOA: semiconductor optical amplifier). Reproduced with permission from [63].

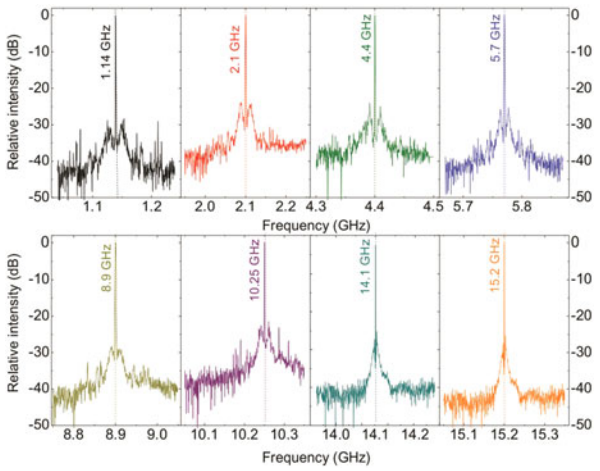


Fig. 18. Offset locking at frequencies up to 15.2 GHz, showing the locking range of the OPLL system using InP-PIC.

fairly open even at 40 Gbps, exhibiting superior performance of error-free ($\mathrm{BER} < 10^{-12}$) up to 35 Gbps. For long propagation through 75 km and 100 km of optical fiber, the eye diagrams of the received 10 Gbps BPSK data are shown in Fig. 16(d).

Recently, chip-scale optical frequency synthesizers are of significant research interest for enabling a number of potential applications, including optical spectroscopy, LiDAR, and optical frequency metrology. There have been ongoing extensive efforts among the scientific community to develop such highly-integrated optical frequency synthesis systems [60]–[62].

Very recently, the experimental demonstration of a chip-scale optical frequency synthesizer was reported [63], [64]. One of the key building blocks in such synthesizers was InP-based PICs that include widely-tunable LO-laser, input waveguide for the light injection from the master oscillator (MO), couplers and on-chip high-speed photodetectors (PDs), monolithically integrated. The system was developed by offset phase-locking the on-chip widely tunable SG-DBR laser to a magnesium fluoride ($MgF_2$) microresonator-based optical frequency comb

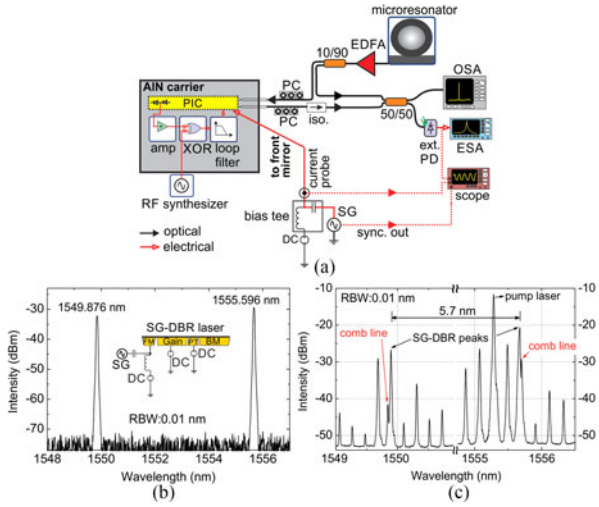


Fig. 19. (a) The test setup for measuring the switching speed of our OFS, (b) the optical spectrum of SG-DBR laser when the current into the front mirror is modulated to result wavelength switching of 5.7 nm, and (c) superimposed optical spectra of comb output and SG-DBR laser, where both comb peaks separated by 0.024 nm from their corresponding SG-DBR laser peaks can be resolved. (BM = back mirror, DC = direct current, EDFA = erbium doped fiber amplifier, ext. PD = external photodetector, FM = front mirror, PIC = photonic integrated circuit, PC = polarization controller, PT = phase tuner, RBW = resolution bandwidth). Reproduced with permission from [63].

using OPLL technology. Fig. 17 shows the experimental setup used in this study to confirm the phase-locking the SG-DBR laser in the InP-PIC to the optical comb. Despite the tuning range of the on-chip laser was ∼50 nm, the coverage of the synthesizer was limited by the comb span, defined by the comb lines intensity exceeding -50 dBm. The balanced PDs integrated in the InP-PIC were mainly responsible for generating differential phase error signals between the SG-DBR laser and a particular comb line to be locked to.

In order to achieve the continuous tuning between comb lines, the developed synthesizer system had a bandwidth exceeding half of the comb's free-spectral-range (FSR). Thus any desired optical frequencies between comb lines could be generated. This was experimentally verified by determining the offset locking range of the heterodyne OPLL system. Fig. 18 shows the RF spectra of the phase-locked on-chip laser with various offsets. By changing the RF reference frequency, the SG-DBR frequency was shifted with an offset up to a frequency of 15.2 GHz relative to the comb line and the heterodyne OPLL phase locked the LO laser to the comb.

It was also demonstrated that the SGDBR output could jump from being locked to one comb line to another many comb lines away. For that, the current into the front mirror in the laser was modulated by a square wave signal with a frequency of 800 kHz and 50% duty cycle. The square-wave signal into the front mirror modulates the lasing wavelength between two values with a separation of ∼5.72 nm (715 GHz), corresponding to 27 comb lines. The wavelength switching rate between these two values was much faster than the spectrum capturing rate the optical spectrum analyzer (OSA). Therefore, both wavelength values on the OSA are observed simultaneously, as shown in Fig. 19(b). The dc offset and amplitude of the square wave were set to

values that result in two output wavelengths of SG-DBR lasers. In order to measure the switching speed, the output wavelengths of the laser beat against two comb lines, generating a RF beat note with the same frequency. The superimposed-optical spectra of comb output and laser at these two specific states are shown in Fig. 19(c). By offset phase locking the SG-DBR laser to the comb lines, the complete operation of the optical frequency synthesis was achieved

## VII. Conclusion

InP-PIC technology has matured, expanded and accelerated at a great speed within the last 20 years. Its technological capability is progressed in a way that can impact every field imaginable. This advancement is primarily made by monolithically integrating and then successfully demonstrating a wide range of photonic functions on the same chip. In addition to the development of high-performance next generation telecom/datacom transceivers, the scientific community is focusing on the realization of InP PIC-based complicated and useful photonic systems that can enable lots of real-world applications in the areas including sensing, imaging and high-speed signal processing.

Despite this advancement of InP-PIC technology, further efforts are still required to reduce the assembly complexity of InP-PICs. Since InP-PICs often are interfaced with electronics and other integrated optical and micro-optical systems, this necessitates a flexible packaging technology that can handle not only low-cost and high-volume demands, but also high-performance components. Hybrid packaging is one of the most popular ways to combine the processed chips in a package and/or on an interposer. On-chip integration of InP-PICs and CMOS electronics is another important area of research that promises to provide a high-performance system with a greatly reduced cost.

A number of InP-based foundry platforms are already established and the open access to these foundries facilitates the development of novel photonic ASICs. With all these past, current and future efforts, it is certain that this InP-PIC technology will move further ahead in the next decade or so. Beyond the areas of telecom and datacom, this maturing technology and its fast advances are then expected to influence our daily lives and socio-economic infrastructure.

## References


[1] D. F. Welch *et al.*, "The realization of large-scale photonic integrated circuits and the associated impact on fiber-optic communication systems," *J. Lightw. Technol.*, vol. 24, no. 12, pp. 4674–4683, Dec. 2006.

[2] L. A. Coldren *et al.*, "High performance InP-based photonic ICs—A tutorial," *J. Lightw. Technol.*, vol. 29, no. 4, pp. 554–570, Feb. 2011.

[3] K. Kudo *et al.*, "1.55-$\mu$m wavelength-selectable microarray DFB-LD's with monolithically integrated MMI combiner, SOA, and EA-modulator," *IEEE Photon. Technol. Lett.*, vol. 12, no. 3, pp. 242–244, Mar. 2000.

[4] P. Bernasconi *et al.*, "Monolithically integrated 40-Gb/s switchable wavelength converter," *J. Lightw. Technol.*, vol. 24, no. 1, pp. 71–76, Jan. 2006.

[5] B. Mason, J. Barton, G. A. Fish, L. A. Coldren, and S. P. DenBaars, "Design of sampled grating DBR lasers with integrated semiconductor optical amplifiers," *IEEE Photon. Technol. Lett.*, vol. 12, no. 7, pp. 762–764, Jul. 2000.

[6] D. Tsou, S. Zaytseva, A. Paucharda, S. Hummela, and Y.-H. Lo, "InP-based three-dimensional photonic integrated circuits," in *Proc. SPIE, Adv. Microelectron. Device Technol.*, 2001, vol. 4600, pp. 10–13.

[7] M. R. Gokhale *et al.*, "Uncooled, 10 Gb/s 1310 nm electroabsorption modulated laser," in *Proc. Opt. Fiber Commun.*, Atlanta, GA, USA, Mar. 2003, p. PD42-P1-3.

[8] J. W. Raring *et al.*, "40 Gbit/s photonic receivers integrating UTC photodiodes with high- and low-confinement SOAs using quantum well intermixing and MOCVD regrowth," *Electron. Lett.*, vol. 42, no. 16, pp. 942–943, 2006.

[9] T. Spuesens *et al.*, "Improved design of an InP-based microdisk laser heterogeneously integrated with SOI," in *Proc. Group IV Photon.*, San Francisco, CA, USA, Sep. 2009, pp. 202–204.

[10] D. Liang *et al.*, "Optimization of hybrid silicon microring lasers," *IEEE Photon. J.*, vol. 3, no. 3, pp. 580–587, Jun. 2011.

[11] G. Kurczveil *et al.*, "An integrated hybrid silicon multiwavelength AWG laser," *IEEE J. Sel. Topics Quantum Electron.*, vol. 17, no. 6, pp. 1521–1527, Nov./Dec. 2011.

[12] S. Srinivasan *et al.*, "Hybrid silicon devices for energy-efficient optical transmitters," *IEEE Micro*, vol. 33, no. 1, pp. 22–31, Jan./Feb. 2013.

[13] J. M. Fedeli *et al.*, "Silicon photonics transceivers with InP on Si lasers," *Mater. Res. Soc.*, vol. 1559, pp. 1–11, 2013.

[14] LightCounting, "Integrated optical devices," Rep., 2017. [Online]. Available: https://www.lightcounting.com/Silicon.cfm

[15] P. R. A. Binetti *et al.*, "Indium phosphide photonic integrated circuits for coherent optical links," *IEEE J. Quantum Electron.*, vol. 48, no. 2, pp. 279–291, Feb. 2012.

[16] G. Gilardi and M. K. Smit, "Generic InP-based integration technology: Present and prospects [invited]," *Prog. Electromagn. Res.*, vol. 147, pp. 23–35, 2014.

[17] M. Smit *et al.*, "An introduction to InP-based generic integration technology," *Semicond. Sci. Technol.*, vol. 29, no. 8, 2014, Art. no. 083001.

[18] K. A. Williams *et al.*, "InP photonic circuits using generic integration [invited]," *Photon. Res.*, vol. 3, no. 5, pp. B60–B68, 2015.

[19] K. Ławniczuk *et al.*, "Open access to technology platforms for InP-based photonic integrated circuits," *Adv. Opt. Technol.*, vol. 4, no. 2, pp. 157–165, 2015.

[20] M. Lauermann *et al.*, "Multi-channel, widely-tunable coherent transmitter and receiver PICs operating at 88 Gbaud/16-QAM," in *Proc. Opt. Fiber Commun.*, Los Angeles, CA, USA, Mar. 2017, pp. 1–3.

[21] J. H. Marsh, "Quantum well intermixing revolutionizes high power laser diodes," *Laser Technik J.*, vol. 4, no. 5, pp. 32–35, 2007.

[22] L. Hou and J. H. Marsh, "Photonic integrated circuits based on quantum well intermixing techniques," *Procedia Eng.*, vol. 140, pp. 107–114, 2016.

[23] M. Aoki *et al.*, "Novel structure MQW electroabsorption modulator/DFB-laser integrated device fabricated by selective area MOCVD growth," *Electron. Lett.*, vol. 27, no. 23, pp. 2138–2140, 1991.

[24] [Online]. Available: https://www.lumentum.com

[25] S. Lange *et al.*, "100 GBd intensity modulation and direct detection with an InP-based monolithic DFB laser Mach-Zehnder modulator," in *Proc. Opt. Fiber Commun.*, Los Angeles, CA, USA, Mar. 2017, pp. 1–3.

[26] N. P. Kelly, L. Caro, M. Dernaika, and F. H. Peters, "Regrowth-free integration of injection locked slotted laser with an electroabsorption modulator," *Opt. Express*, vol. 25, no. 4, pp. 4054–4060, Feb. 20, 2017.

[27] H. Debrégeas *et al.*, "Record 6dBm electroabsorption modulated laser for 10Gb/s and 25Gb/s high power budget access networks," in *Proc. Opt. Fiber Commun.*, Los Angeles, CA, USA, Mar. 2017, pp. 1–3.

[28] Y. Kawamura, K. Wakita, Y. Itaya, Y. Yoshikuni, and H. Asahi, "Monolithic integration of InGaAsp/InP DFB lasers and InGaAs/InAIAs MQW optical modulators," *Electron. Lett.*, vol. 22, no. 5, pp. 242–243, 1986.

[29] M. Suzuki *et al.*, "Monolithic integration of InGaAsP/InP distributed feedback laser and electroabsorption modulator by vapor phase epitaxy," *J. Lightw. Technol.*, vol. LT-5, no. 9, pp. 1277–1285, Sep. 1987.

[30] Y. Akulova, "InP photonic integrated circuits for high efficiency pluggable optical interfaces," in *Proc. Opt. Fiber Commun.*, Los Angeles, CA, USA, Mar. 2015, pp. 1–3.

[31] Y. Akulova, "InP photonic integrated circuits for high efficiency optical transceivers," in *Proc. IEEE Photon. Conf.*, San Diego, CA, USA, Oct. 2014, pp. 1–2.

[32] V. Lal *et al.*, "Extended C-band tunable multi-channel InP-based coherent transmitter PICs," *J. Lightw. Technol.*, vol. 35, no. 7, pp. 1320–1327, Apr. 2017.

[33] Y. Akulova, "Advances in integrated widely tunable coherent transmitters," in *Proc. Opt. Fiber Commun.*, Anaheim, CA, USA, Mar. 2016, pp. 1–3.

[34] M. Larson *et al.*, "Narrow linewidth sampled-grating distributed Bragg reflector laser with enhanced side-mode suppression," in *Proc. Opt. Fiber Commun.*, Los Angeles, CA, USA, Mar. 2015, pp. 1–3.
[35] G. B. Morrison *et al.*, "Optoelectronic transmitter design to enable RF photonic systems," in *Proc. Int. Topical Meeting Microw. Photon.*, Long Beach, CA, USA, Nov. 2016, pp. 325–327.
[36] M. L. Mashanovitch *et al.*, "A novel widely tunable monolithically integrated transmitter device in indium phosphide," in *Proc. Adv. Photon. IPR*, 2017, Paper IM3A.3.
[37] X. Xiaobo, J. Khurgin, K. Jin, and F. S. Chow, "Linearized Mach-Zehnder intensity modulator," *IEEE Photon. Technol. Lett.*, vol. 15, no. 4, pp. 531–533, Apr. 2003.
[38] E. J. Norberg, R. S. Guzzon, S. C. Nicholes, J. S. Parker, and L. A. Coldren, "Programmable photonic lattice filters in InGaAsP-InP," *IEEE Photon. Technol. Lett.*, vol. 22, no. 2, pp. 109–111, Jan. 2010.
[39] J. S. Fandiño, P. Muñoz, D. Doménech, and J. Capmany, "A monolithic integrated photonic microwave filter," *Nature Photon.*, vol. 11, no. 2, pp. 124–129, 2016.
[40] E. J. Norberg, R. S. Guzzon, J. S. Parker, L. A. Johansson, and L. A. Coldren, "Programmable photonic microwave filters monolithically integrated in InP-InGaAsP," *J. Lightw. Technol.*, vol. 29, no. 11, pp. 1611–1619, Jun. 2011.
[41] R. S. Guzzon, E. J. Norberg, and L. A. Coldren, "Spurious-free dynamic range in photonic integrated circuit filters with semiconductor optical amplifiers," *IEEE J. Quantum Electron.*, vol. 48, no. 2, pp. 269–278, Feb. 2012.
[42] W. Liu *et al.*, "A fully reconfigurable photonic integrated signal processor," *Nature Photon.*, vol. 10, no. 3, pp. 190–195, 2016.
[43] W. Liu *et al.*, "A photonic temporal integrator with an ultra-long integration time window based on an InP-InGaAsP integrated ring resonator," *J. Lightw. Technol.*, vol. 32, no. 20, pp. 3654–3659, Oct. 2014.
[44] W. Jiang *et al.*, "A monolithic InP-based photonic integrated circuit for optical arbitrary waveform generation," in *Proc. Opt. Fiber Commun.*, San Diego, CA, USA, Feb. 2008, pp. 1–3.
[45] F. M. Soares *et al.*, "Monolithic InP 100-channel $\times$ 10-GHz device for optical arbitrary waveform generation," *IEEE Photon. J.*, vol. 3, no. 6, pp. 975–985, Dec. 2011.
[46] M. J. R. Heck, "Highly integrated optical phased arrays: Photonic integrated circuits for optical beam shaping and beam steering," *Nanophotonics*, vol. 6, no. 1, pp. 93–107, 2017.
[47] W. Guo *et al.*, "InP photonic integrated circuit for 2D optical beam steering," in *Proc. Int. Photon. Nanofabrication Test.*, Wuhan, China, Nov. 2012, pp. 1–2.
[48] W. Guo, P. R. A. Binetti, C. Althouse, L. A. Johansson, and L. A. Coldren, "InP photonic integrated circuit with on-chip tunable laser source for 2D optical beam steering," in *Proc. Opt. Fiber Commun.*, Anaheim, CA, USA, Mar. 2013, pp. 1–3.
[49] W. Guo *et al.*, "Two-dimensional optical beam steering with InP-based photonic integrated circuits," *IEEE J. Sel. Topics Quantum Electron.*, vol. 19, no. 4, Jul./Aug. 2013, Art. no. 6100212.
[50] J. K. Doylend *et al.*, "Two-dimensional free-space beam steering with an optical phased array on silicon-on-insulator," *Opt. Express*, vol. 19, no. 22, pp. 21595–21604, 2011.
[51] S. J. M. Paul, J. Bowers, L. A. Coldren, and S. J. B. Yoo, "Photonic integrated circuits for coherent LiDAR," in *Proc. 18th Coherent Laser Radar Conf.*, Boulder, CO, USA, 2016, Paper T12.
[52] A. Sivananthan *et al.*, "Integrated linewidth reduction of a tunable SG-DBR laser," in *Proc. Conf. Lasers Electro-Opt.*, 2013, Paper CTu1L.2.
[53] A. Sivananthan *et al.*, "Monolithic linewidth narrowing of a tunable SG-DBR laser," in *Proc. Opt. Fiber Commun.*, Anaheim, CA, USA, Mar. 2013, pp. 1–3.
[54] B. Song, C. Stagarescu, S. Ristic, A. Behfar, and J. Klamkin, "3D integrated hybrid silicon laser," *Opt. Express*, vol. 24, no. 10, pp. 10435–10444, 2016.
[55] B. Song *et al.*, "3D integrated hybrid silicon laser," in *Proc. Eur. Conf. Opt. Commun.*, Valencia, Spain, Sep. 2015, pp. 1–3.
[56] B. Song, L. Megalini, S. Dwivedi, S. Ristic, and J. Klamkin, "High thermal performance 3D hybrid silicon lasers," *IEEE Photon. Technol. Lett.*, vol. 29, no. 14, pp. 1143–1146, Jul. 2017.
[57] B. Song, Y. Liu, S. Ristic, and J. Klamkin, "Tunable 3D hybrid integrated silicon photonic external cavity laser," in *Proc. Conf. Lasers Electro-Opt.*, San Jose, CA, USA, May 2017, pp. 1–2.
[58] H.-C. Park *et al.*, "40 Gbit/s coherent optical receiver using a Costas loop," *Opt. Express*, vol. 20, no. 26, pp. B197–B203, 2012.
[59] M. Lu *et al.*, "An integrated 40 Gbit/s optical Costas receiver," *J. Lightw. Technol.*, vol. 31, no. 13, pp. 2244–2253, Jul. 2013.
[60] J. E. Bowers *et al.*, "Chip-scale optical resonator enabled synthesizer (CORES) miniature systems for optical frequency synthesis," in *Proc. IEEE Int. Freq. Control Symp.*, New Orleans, LA, USA, Sep. 2016, pp. 1–5.
[61] M. Lu *et al.*, "A highly-integrated optical frequency synthesizer based on phase-locked loops," in *Proc. Opt. Fiber Commun.*, San Francisco, CA, USA, Mar. 2014, pp. 1–3.
[62] D. T. Spencer *et al.*, "Towards an integrated photonics optical-frequency synthesizer with $<$1 Hz residual frequency noise," in *Proc. Opt. Fiber Commun.*, Los Angeles, CA, USA, Mar. 2017, pp. 1–3.
[63] S. Arafin *et al.*, "Towards chip-scale optical frequency synthesis based on optical heterodyne phase-locked loop," *Opt. Express*, vol. 25, no. 2, pp. 681–695, 2017.
[64] S. Arafin *et al.*, "Power-efficient Kerr frequency comb based tunable optical source," *IEEE Photon. J.*, vol. 9, no. 3, Jun. 2017, Art. no. 6600814.

**Shamsul Arafin** (S'08–M'12–SM'17) received the B.Sc. degree in electrical and electronics engineering from Bangladesh University of Engineering and Technology, Dhaka, Bangladesh, in 2005, the M.Sc. degree in communication technology from Universität Ulm, Ulm, Germany, in 2008, and the Ph.D. degree from the Walter Schottky Institut, Technische Universität München, Munich, Germany, in 2012. He is currently an Assistant Project Scientist at the University of California, Santa Barbara (UCSB), Santa Barbara, CA, USA. Prior to joining UCSB, he was a Postdoctoral Research Scholar in Device Research Laboratory, University of California, Los Angeles, CA, USA. He has authored and coauthored more than 80 papers in leading technical journals and international conferences.

**Larry A. Coldren** (S'67–M'72–SM'77–F'82–LF'12) received the Ph.D degree in electrical engineering from Stanford University, Stanford, CA, USA, in 1972. After 13 years in the research area with Bell Laboratories, he joined the University of California at Santa Barbara (UCSB) in 1984. He is currently the Fred Kavli Professor of optoelectronics and sensors and holds appointments with the Department of Materials and the Department of Electrical and Computer Engineering. From 2009 to 2011, he was acting Dean of the College of Engineering. In 1990, he cofounded Optical Concepts, later acquired as Gore Photonics, to develop novel VCSEL technology, and, in 1998, he cofounded Agility Communications, later acquired by JDSU (now Lumentum), to develop widely tunable integrated transmitters. At UCSB, he worked on multiple-section widely tunable lasers and efficient vertical-cavity surface-emitting lasers (VCSELs). More recently, his group has developed high-performance InP-based photonic integrated circuits and high-speed, high-efficiency VCSELs. He has authored or coauthored more than a thousand journal and conference papers, eight book chapters, a widely used textbook, and 63 issued patents. He is a Fellow of OSA, IEE, and the National Academy of Inventors, as well as a member of the National Academy of Engineering. He received the 2004 John Tyndall Award, the 2009 Aron Kressel Award, the 2014 David Sarnoff Award, the 2015 IPRM Award, and the 2017 Nick Holonyak, Jr. Award.